PHYSICAL REVIEW D **84,** 115009 (2011)

Production of long-lived staus in the Drell-Yan process

Jan Heisig* and Jörn Kersten†

II. Institute for Theoretical Physics, University of Hamburg, Luruper Chaussee 149, 22761 Hamburg, Germany

(Received 13 September 2011; published 9 December 2011)

We investigate the phenomenology of the gravitino dark matter scenario with a stau as the next-to-lightest supersymmetric particle at the LHC. For a wide range of gravitino masses the lighter stau is stable on the scale of a detector and gives rise to a prominent signature as a "slow muon." The direct stau production via the Drell-Yan process is always present and independent of the mass spectrum of the other superparticles, thus providing a lower bound for the discovery potential of this scenario. Performing a careful analysis with particular emphasis on the criteria for observing stau pairs and for distinguishing them from the background, we find that the 14 TeV run of the LHC has a promising potential for finding long-lived staus from Drell-Yan production up to very large stau masses.

DOI: 10.1103/PhysRevD.84.115009 PACS numbers: 12.60.Jv, 14.80.Ly

I. INTRODUCTION

Supersymmetry (SUSY) with conserved R-parity and a gravitino as the lightest superparticle (LSP) is a viable alternative to the most widely studied scenario with a neutralino LSP. A stable gravitino is a perfectly good dark matter candidate [1,2] and may even be regarded as favored, since it alleviates the cosmological gravitino problem, allowing for a higher reheating temperature after inflation [3,4]. As the superpartner of the graviton, the gravitino takes part only in the gravitational interaction. Therefore, the next-to-LSP (NLSP) is typically quite long-lived.[1] For a charged NLSP, this leads to a spectacular signature at colliders, charged tracks leaving the detector and no missing transverse energy. It could even be possible to capture NLSPs and to study their decays in detail, thus measuring the strength of their coupling to the LSP and the LSP's spin [7]. In this way, observations of the NLSP could lead to an indirect determination of the nature of the LSP.

In this work, we consider a charged slepton NLSP. In the following, we refer to the lightest charged slepton as the stau $\tilde{\tau}_1$ and allow for mixing between $\tilde{\tau}_R$ and $\tilde{\tau}_L$, the superpartners of the right- and left-handed tau, respectively. Of course, the results are also valid for a selectron or smuon NLSP. For a wide range of gravitino and stau masses, the stau NLSP lifetime

$$\tau_{\tilde{\tau}} \simeq 6 \times 10^4 \mathrm{s} \left(\frac{m_{3/2}}{\mathrm{GeV}}\right)^2 \left(\frac{m_{\tilde{\tau}}}{100\ \mathrm{GeV}}\right)^{-5} \tag{1}$$

is larger than about 10^{-7} s. Then the stau is metastable, i.e., it usually leaves an LHC detector before decaying.

*jan.heisig@desy.de
†joern.kersten@desy.de

[1] The same is true in scenarios with an axino LSP, whose interactions are strongly suppressed by the large Peccei-Quinn scale, see, e.g., [5]. The NLSP can also be long-lived if its mass is very close to that of a neutralino LSP [6]. We do not study these alternatives in detail but expect the same results as in the case considered.

In this scenario catalyzed big bang nucleosynthesis [8] leads to an upper bound of roughly 10^4 s on the stau lifetime. While this bound can in principle be satisfied by lowering the gravitino mass sufficiently, a short lifetime is also obtained for gravitino masses in the GeV range and a relatively heavy stau [9,10] due to the dependence of $\tau_{\tilde{\tau}}$ on $m_{\tilde{\tau}_1}^{-5}$.

Previous studies of the LHC phenomenology of metastable staus have concentrated on the production via decays of heavier superparticles, assuming specific scenarios for SUSY breaking [11–26]. See also [27] for a comprehensive review of the topic. Here we do not restrict ourselves to a specific SUSY-breaking scenario, and we focus on the direct production of staus via the neutral current Drell-Yan (DY) process, which possesses interesting properties:

(i) The DY contribution is independent of all parameters of the Minimal Supersymmetric Standard Model (MSSM) except $m_{\tilde{\tau}_1}$ and the stau mixing angle $\theta_{\tilde{\tau}}$, enabling a model-independent analysis.

(ii) The DY process is always present. Together with the previous point, conservatively this leads to an assured discovery potential and strict exclusion limits in a class of scenarios characterized only by $m_{\tilde{\tau}_1}$ and $\theta_{\tilde{\tau}}$.

Thus, it is natural to ask for the required luminosity which provides this robust exclusion limit (and the discovery reach) in the 7 TeV and 14 TeV LHC run. Although the DY production of staus has been included in some studies [26,28,29], the focus of these works has been different and—to our knowledge—this question has only been addressed in a brief remark in the review [30], where the aim is only a rough estimate with fairly conservative assumptions. Here, we perform a careful analysis, in particular, examining the dependence on the imposed cuts and using the proper statistics for small event numbers. We also take into account the latest information from the LHC experiments on discriminating heavy stable charged particles from muons. We find that the opposite-sign stau pair from DY production allows for a clean signal region up to very large integrated luminosities. Thus, in spite of its small cross section the DY process is able to provide an interesting discovery and exclusion potential, even for relatively large stau masses and significantly better than estimated in [30].

The paper is organized as follows. In Sec. II we examine the DY process, discussing the criteria for observing stau pairs and for distinguishing them from the background. This allows us to derive the LHC's discovery reach and exclusion potential in Sec. III. In Sec. IV we briefly compare DY production with the production of staus from the decay of heavier superparticles. The purpose of this consideration is to estimate for which SUSY spectra the exclusion limit from direct DY production is tight and for which spectra it tends to be overly loose. We will see that the direct DY production can be dominant for large mass gaps between the stau NLSP and the colored superparticles. Unless noted otherwise, we discuss the 14 TeV LHC run in what follows.

II. STAUS FROM THE DRELL-YAN PROCESS

Let us first discuss in detail the DY production of staus, the expected signal in a detector at the LHC and the background suppression. All events have been generated with MADGRAPH/MADEVENT 4 [31] and its PYTHIA [32] interface. For the event generation in MADEVENT and PYTHIA we enabled the MLM matching scheme [33]. The CTEQ6L1 PDF set [34] has been used.

A. Background

Staus as heavy metastable charged particles usually leave the detector. This leads to a signal in the tracker and muon chambers. Muons are the only background. Therefore, we first study this background in order to devise suitable cuts, which we can then take into account in the calculation of the signal in the next subsection.

The di-muon rate for the moderate and high p_T range is much smaller than the single muon rate, and the possible sources are considerably fewer in the case of di-muons. For a p_T cut smaller and around 15 GeV, b and c decays are the dominant sources of di-mouns. Above 15 GeV the DY production begins to dominate [35]. In addition to a high p_T cut, the b and c contributions can be further reduced by isolation cuts. This feature relies on the fact that b and c quarks are always produced close to jets while muons from heavy mother particles (like Z or t) tend to be well separated from the other decay products—they are isolated [36].

As preselection cuts on the data, we require two opposite-sign muonlike particles each satisfying

(i) p_T cut: $p_T > 50$ GeV,

(ii) Barrel cut on the pseudorapidity: $|\eta| < 2.5$,

(iii) Isolation cut: $\Delta\mathcal{R}_{\mu,\mathrm{jet}} = \sqrt{\Delta\eta^2_{\mu,\mathrm{jet}} + \Delta\phi^2_{\mu,\mathrm{jet}}} > 0.5$ for jets with $p_T > 50$ GeV.

With the p_T and the isolation cut, a sufficient rejection of the b and c contributions should easily be obtained. This is why we refrain from running a detector simulation for this issue. All the same we made no effort to specify the isolation algorithm. Instead we apply the respective cuts directly on the remaining background (and signal) at the level of the PYTHIA Les Houches Event output. The p_T cut also rejects muon pairs from on shell Z decay. Therefore, an additional cut on the invariant mass of the muon pair, which was used in [28], would not have a significant effect.

As the remaining background, we consider di-muons from the DY process and from $t\bar{t}$ production. We include contributions up to order α_s^2 (two jets) in the case of the DY process and α_s^3 (three jets) in the case of $t\bar{t}$ production and generate 2×10^5 unweighted events for the analysis. The total normalization of the cross section was fixed from the leading-order DY di-muon production (without jets) from MADEVENT multiplied by a constant K factor, conservatively chosen to be 1.4, to account for next-to-leading order (NLO) corrections. The total di-muon cross section after applying the above preselection cuts is then $\sigma_B \simeq 25$ pb.

Velocity measurement

The crucial tool for distinguishing muons from staus is the velocity measurement. A significant fraction of staus with a mass of several hundred GeV will have a velocity well below the speed of light, whereas the background muons are always ultrarelativistic. Unfortunately, measuring the velocity is much more involved than measuring, for example, the momentum. Therefore, the experimental uncertainty is much larger, and a cut on the velocity will not reject all background muons.

There are two distinct ways of measuring the velocity of muonlike particles, the ionization energy loss (dE/dx) inside the tracker and the time-of-flight (ToF) measurement, which measures the time between the bunch crossing and the passing through the muon chambers. The former measurement only provides information up to $\beta \lesssim 0.9$ while the latter is mainly limited from below—at the design luminosity of the LHC, particles with velocities less than about 0.6 cannot be assigned to the correct bunch crossing anymore.

Although the precision of each velocity measurement is not overwhelming, a combination of both measurements provides a highly efficient background rejection. This is due to the fact that for stau signal events these two measurements are clearly correlated while for background events no correlation is present [37]. According to [38] a cut using both measurements, $\beta_{dE/dx}$, $\beta_{\mathrm{ToF}} < 0.8$, leads to a background rejection factor of about 10^{-7} for single stau candidates.

Thus, if the probability of a misidentification of two muons within one event is not correlated, a background rejection factor of $r_\beta = 10^{-14}$ could be achievable.[2]

[2] A possible source of such a correlation would be the presence of a highly correlated η^+-η^- distribution together with a strong dependence of the velocity resolution function on η. However, Fig. 1 shows that already the former is not the case.

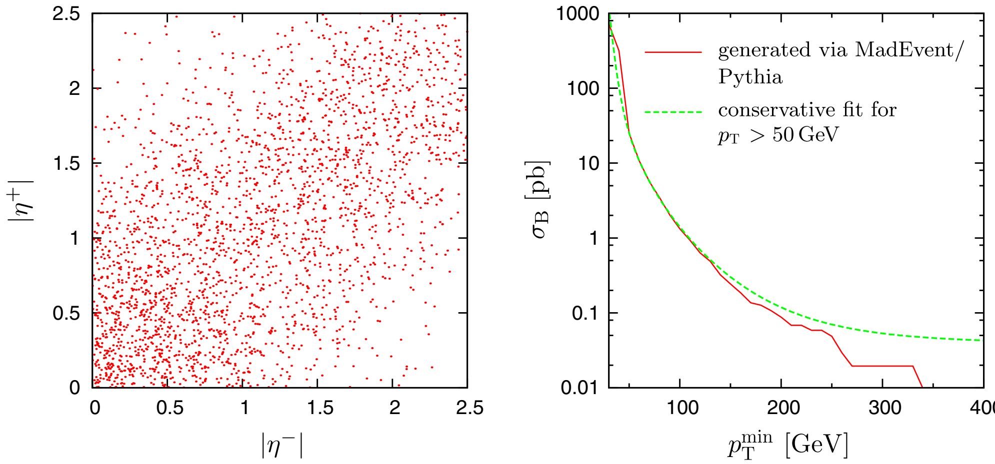

FIG. 1 (color online). Left: Pseudorapidity distribution of the considered di-muon background after applying the preselection cuts, where $\eta^{\pm}$ denotes the pseudorapidity of $\mu^{\pm}$. Right: Total di-muon cross section after applying the preselection cuts but as a function of the variable p_T cut discussed at the end of Sec. III (again on both muons). Both plots are valid for the 14 TeV LHC.

However, for $r_\beta = 10^{-14}$, the relevant background appears only at very high luminosities, when pileup from different bunch crossings becomes relevant. This fact might lower the background rejection with respect to the naïve expectation of $r_\beta = 10^{-14}$. To our knowledge, currently no quantitative study exists about this issue. In any case, we shall see later that a sufficient background rejection (which enables a three-event exclusion over the whole considered region for $m_{\tilde{\tau}_1}$) can already be achieved with $r_\beta \simeq 10^{-10}$. Thus, using this value is both sufficient and conservative. To show the effect of a looser background rejection we will also display the results under the pessimistic assumption that we do not gain anything by requiring *two* stau candidates, hence applying $r_\beta = 10^{-7}$.

Following these considerations, we will apply the cuts $0.6 < \beta < 0.8$ on the signal events in order to ensure both a working ToF measurement and a sufficient background rejection.

B. Signal

The direct stau production via DY only involves two parameters of the more than 100 free MSSM parameters, the stau mass $m_{\tilde{\tau}_1}$ and the mixing angle $\theta_{\tilde{\tau}}$.

1. Dependence on the mixing angle

We define the stau mixing matrix via

$$\begin{pmatrix} \tilde{\tau}_1 \\ \tilde{\tau}_2 \end{pmatrix} = \mathcal{M}^{\tilde{\tau}} \begin{pmatrix} \tilde{\tau}_R \\ \tilde{\tau}_L \end{pmatrix} = \begin{pmatrix} \cos\theta_{\tilde{\tau}} & \sin\theta_{\tilde{\tau}} \\ -\sin\theta_{\tilde{\tau}} & \cos\theta_{\tilde{\tau}} \end{pmatrix} \begin{pmatrix} \tilde{\tau}_R \\ \tilde{\tau}_L \end{pmatrix} \quad (2)$$

and $m_{\tilde{\tau}_1} \leq m_{\tilde{\tau}_2}$. The dependence of the di-stau cross section on the mixing angle $\theta_{\tilde{\tau}}$ can be discussed by considering the tree-level parton-level cross section for $q\bar{q} \to Z, \gamma \to \tilde{\tau}_i^+ \tilde{\tau}_j^-$,

$$\left(\frac{d\hat{\sigma}}{d\hat{t}}\right)^q_{ij} = \frac{e^4}{8\pi} \frac{\hat{u}\,\hat{t} - m^2_{\tilde{\tau}_i} m^2_{\tilde{\tau}_j}}{\hat{s}^4} \Bigg[Q_q^2 \delta_{ij} + (g_V^{q2} + g_A^{q2}) \times \frac{g^2_{\tilde{\tau}_i\tilde{\tau}_j}}{(1 - M_Z^2/\hat{s})^2} - \frac{2Q_q g_V^q \delta_{ij} g_{\tilde{\tau}_i\tilde{\tau}_j}}{1 - M_Z^2/\hat{s}} \Bigg], \quad (3)$$

where

$$g_{\tilde{\tau}_i\tilde{\tau}_j} = \frac{1}{c_W s_W} \Bigg[\left(-\frac{1}{2} + s_W^2 \right) \mathcal{M}^{\tilde{\tau}}_{iL} \mathcal{M}^{\tilde{\tau}}_{jL} + s_W^2 \mathcal{M}^{\tilde{\tau}}_{iR} \mathcal{M}^{\tilde{\tau}}_{jR} \Bigg] \quad (4)$$

and

$$g_V^q = \frac{T_q^3 - 2Q_q s_W^2}{2c_W s_W}, \qquad g_A^q = \frac{T_q^3}{2c_W s_W}. \quad (5)$$

Here q denotes the flavor of the annihilating quark, while Q_q and T_q^3 are its electric charge and the third component of its weak isospin, respectively. Besides, $c_W \equiv \cos\theta_W$, $s_W \equiv \sin\theta_W$, and $\hat{s}$, $\hat{t}$, $\hat{u}$ are the Mandelstam variables. (Taking into account the width $\Gamma_Z \ll M_Z$ is not vital for the following argumentation.)

A change in $\theta_{\tilde{\tau}}$ has an impact on $g_{\tilde{\tau}_i\tilde{\tau}_j}$ only. Thus, it alters the ratio between the three terms in square brackets in (3), which are the electromagnetic, the weak, and the interference terms, respectively. This change is almost independent of the kinematics. The terms in square brackets contain $\hat{s}$ as the only kinematic variable, and even this dependence becomes negligible when exceeding a few times M_Z. The left panel of Fig. 2 shows the ratio between the first term and all terms in (3) as a function of $\hat{s}$ (arbitrarily normalized). From a few hundred GeV on the ratio is almost constant. Thus, in this region a change in $\theta_{\tilde{\tau}}$ will only shift the overall cross section without any impact on the kinematic distributions. In fact, the dependence of the cross section on $\theta_{\tilde{\tau}}$ shown in the right panel of Fig. 2 is applicable to all stau masses considered in the following.

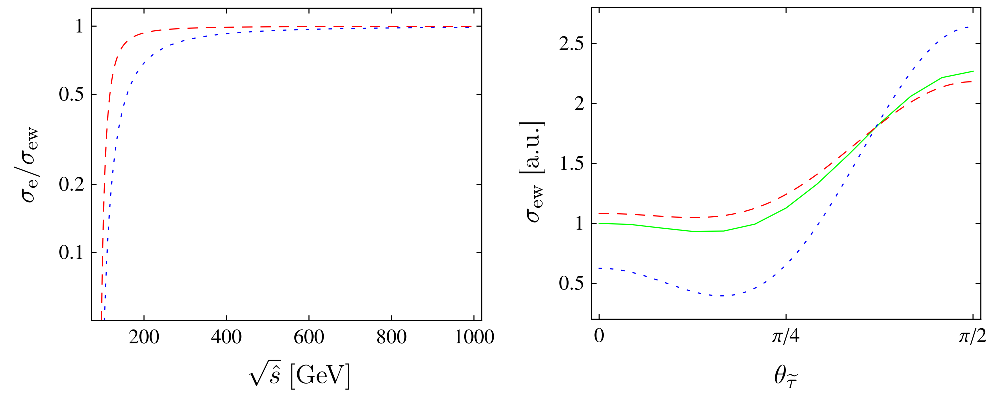

FIG. 2 (color online). Left: Ratio between the electromagnetic contribution and the complete electroweak cross section (3) for $\theta_{\tilde{\tau}} = 0$ as a function of $\sqrt{\hat{s}}$ for up-type quarks (red dashed line) and down-type quarks (blue dotted line). In each case the ratio is normalized to be one at $\hat{s} \to \infty$. Right: Cross section for direct di-stau production $pp \to Z, \gamma \to \tilde{\tau}_1^+ \tilde{\tau}_1^-$ as a function of the stau mixing angle. The curves are obtained from a MADEVENT simulation with $m_{\tilde{\tau}_1} = 500$ GeV (solid green, normalized to be one at $\theta_{\tilde{\tau}} = 0$) as well as directly from (3) for up-type quarks (red dashed line) and down-type quarks (blue dotted line) for a center-of-mass energy $\sqrt{\hat{s}} = 1000$ GeV. The two latter curves are absolutely normalized to be equal to the MADEVENT prediction at their intersection point.

For the plots in Figs. 3 and 4 we consider the case $\theta_{\tilde{\tau}} = 0$. However, the minimum of $\sigma_{ew}(\theta_{\tilde{\tau}})$ is at $\theta_{\tilde{\tau}}^{min} \neq 0$ and it is about 7% lower than the value at $\sigma_{ew}(0)$. Therefore, when estimating the discovery potential and exclusion limits we conservatively choose $\theta_{\tilde{\tau}} = \theta_{\tilde{\tau}}^{min}$. The limits for other values of $\theta_{\tilde{\tau}}$ can easily be obtained from the displayed curves. Since it turns out that we can achieve a (almost) clean signal region, the required luminosity is, to a very good approximation, simply proportional to the inverse of the cross section.

2. Dependence on the stau mass

To show the dependence on the stau mass $m_{\tilde{\tau}_1}$ we simulated the DY production in 21 mass steps from 100 GeV to 1000 GeV, generating 5×10^4 events for each one and again considering diagrams up to order α_s^2 (two jets). We obtained the normalization of the total cross section from the corresponding leading-order computation (without jets) from MADEVENT, corrected by a constant K factor of 1.35 [39]. This value was found for $m_{\tilde{\tau}_1} \gtrsim$ 200 GeV considering NLO QCD corrections. Additionally including SUSY QCD contributions at NLO and next-to-leading logarithmic accuracy yields a K factor between roughly 1.29 and 1.36 [40–42].

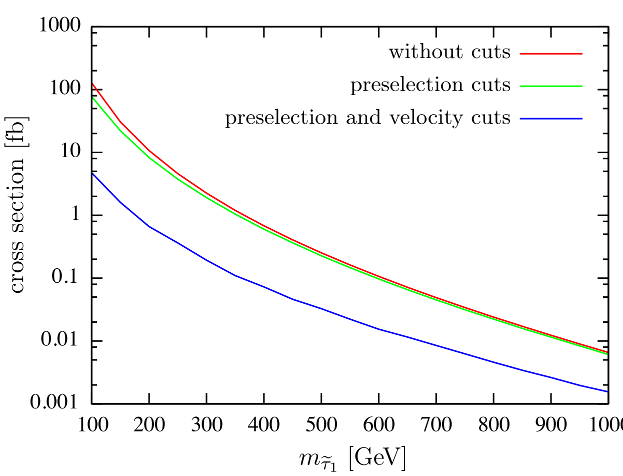

FIG. 3 (color online). Cross section for direct di-stau production $pp \to Z, \gamma \to \tilde{\tau}_1^+ \tilde{\tau}_1^-$ for $\theta_{\tilde{\tau}} = 0$ ($\tilde{\tau}_1 = \tilde{\tau}_R$) as a function of $m_{\tilde{\tau}}$ at the 14 TeV LHC. The impact of the preselection cuts ($|\eta| < 2.5$, $p_T > 50$ GeV, $\Delta\mathcal{R}_{\tilde{\tau},jet} > 0.5$) and the velocity cut ($0.6 < \beta < 0.8$) is displayed.

Figure 3 shows the results. The cuts on η, p_T, and $\Delta\mathcal{R}_{\tilde{\tau},jet}$ have a minor impact on the data, whereas the velocity cut lowers the signal by about 1 order of magnitude but with a slightly decreasing tendency when going to very high masses due to the increase of slower staus. The fraction of events passing the velocity cut is 8% at $m_{\tilde{\tau}_1} =$ 200 GeV and about 20% at $m_{\tilde{\tau}_1} = 800$ GeV (cf. Figure 4, top). This is due to the fact that the parton luminosities in a 14 TeV pp collision begin to decrease more drastically for center-of-mass (CM) energies above roughly 1 TeV. The top panel of Fig. 4 also shows that the velocity cut at $\beta = 0.6$ has considerably less impact on the data than the one at $\beta = 0.8$.

The partonic process considered in (3) favors perpendicular scattering: $(\hat{u}\,\hat{t} - m_{\tilde{\tau}}^4)d\hat{t} \propto \sin^2\theta d\Omega$, where θ is the angle between the produced staus and the beam axis in the CM frame and $d\Omega$ the corresponding solid angle element. Thus, the very low p_T region is suppressed. On the other hand, the faster decrease of the parton luminosity with increasing CM energy determines the high-p_T tail. This leads to a p_T distribution that peaks roughly at $p_T \simeq m_{\tilde{\tau}_1}$, at least for the mass range $m_{\tilde{\tau}_1} \lesssim 400$ GeV. For larger masses the behavior of the parton luminosity at high CM energies shifts this peak a bit downwards (see Fig. 4, bottom). Figure 4, bottom also shows that the p_T distributions of the two staus are clearly correlated.

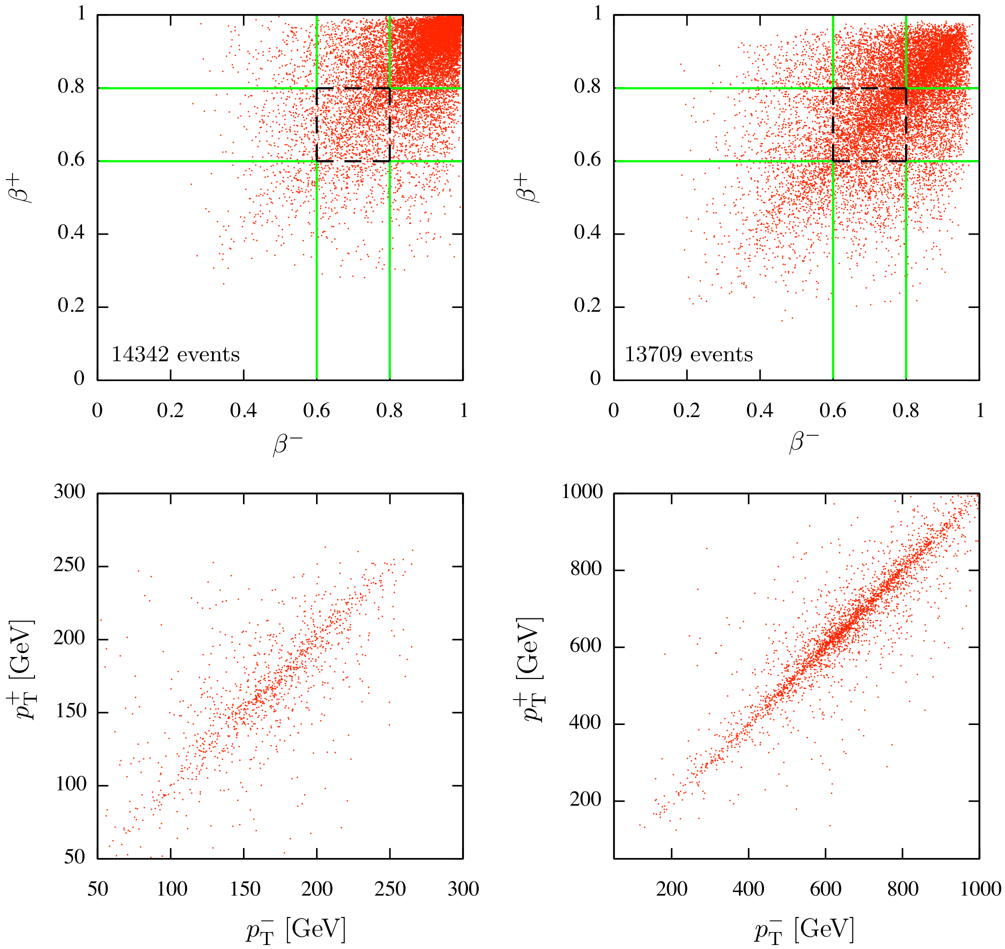

FIG. 4 (color online). Di-stau distributions at the 14 TeV LHC after the preselection cuts for $m_{\tilde{\tau}_1} = 200$ GeV (left) and $m_{\tilde{\tau}_1} = 800$ GeV (right). Top: Unweighted events as dots in the β^--β^+ plane, where $\beta^\pm$ is the velocity of $\tilde{\tau}^\pm$. The black dashed square denotes the region selected by the velocity cut. It contains 1146 (left) and 2824 (right) events. Bottom: Distribution in the p_T^+-p_T^- plane of the events passing the velocity cut.

III. DISCOVERY POTENTIAL AND EXCLUSION LIMITS

In the following we are interested in the integrated luminosity $\mathcal{L}_f(m_{\tilde{\tau}_1})$ required to discover or exclude the considered scenario characterized by the parameter $m_{\tilde{\tau}_1}$. The expectation value for the number of signal events S is given by

$$S = \sigma_S(m_{\tilde{\tau}_1})\mathcal{L}_f\,\epsilon, \tag{6}$$

where $\sigma_S(m_{\tilde{\tau}_1})$ is the signal cross section and ϵ is the detector efficiency. The expected number of background events reads

$$B = \sigma_B r_\beta \mathcal{L}_f, \tag{7}$$

where σ_B is the background cross section and r_β is the background rejection factor due to the velocity discrimination. (Conservatively, we set the detector efficiency for the background to one.)

Since we expect to obtain solutions that involve small event numbers S and B, we consider Poisson statistics. A 5σ discovery corresponds to a set of S and B that fulfills

$$1 - e^{-B}\sum_{n=0}^{B+S-1}\frac{B^n}{n!} \stackrel{!}{=} 3\times 10^{-7}, \tag{8}$$

where 3×10^{-7} is the one-sided p value corresponding to a 5σ evidence.

A 95% C.L. exclusion corresponds to S and B satisfying

$$1 - \frac{e^{-(B+S)}\sum_{n=0}^{N}\frac{(B+S)^n}{n!}}{e^{-B}\sum_{n=0}^{N}\frac{B^n}{n!}} \stackrel{!}{=} 0.95. \tag{9}$$

In contrast to the case of discovery, the additional parameter N appears. This is the maximum observed event number up to which the 95% C.L. exclusion is demanded to hold. For $N = B$ we obtain the central value of the

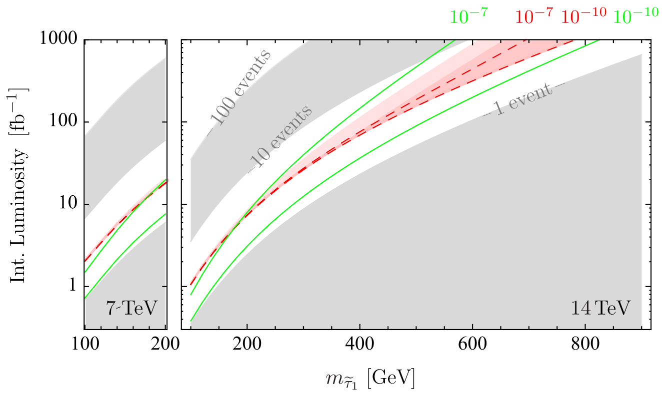

FIG. 5 (color online). Integrated luminosity at which a 5σ discovery (green solid lines) and a 95% C.L. exclusion (red dashed lines) of directly produced stau pairs is to be expected. We have chosen the stau mixing angle $\theta_{\tilde{\tau}}^{\min}$ that yields the smallest production cross section. The dependence on the background rejection factor for the velocity cut is illustrated by displaying each curve for $r_\beta = 10^{-10}$ as well as $r_\beta = 10^{-7}$. The dark and light red-shaded band around the $r_\beta = 10^{-7}$ curve displays the 1σ and 2σ probability band, respectively. The results are shown for the 7 TeV and 14 TeV run of the LHC.

exclusion limit. Repeating the analysis for N at the boundaries of the 1σ and 2σ intervals around B then yields the 1σ and 2σ probability bands for the exclusion limit.

Inserting S and B as functions of $\mathcal{L}_\int$ and $\sigma_{\rm B}$ according to (6) and (7) turns the formulae (8) and (9) into implicit functions determining $\mathcal{L}_\int(m_{\tilde{\tau}_1})$.

As signal cross section we use $\sigma_{\rm S}(m_{\tilde{\tau}_1})$ at $\theta_{\tilde{\tau}} = \theta_{\tilde{\tau}}^{\min}$ after applying all cuts mentioned above. The trigger and reconstruction efficiency for single stau candidates can be conservatively estimated to be 80% [43], thus we choose (again conservatively) $\epsilon = 0.8^2$. The background cross section $\sigma_{\rm B}$ is the di-muon cross section after the preselection cuts. As explained earlier, we consider the values 10^{-10} as well as 10^{-7} for r_β. Figure 5 shows the luminosity $\mathcal{L}_\int(m_{\tilde{\tau}_1})$ at which a 5σ discovery can be expected (green solid lines) and at which all scenarios with a metastable stau can be excluded at 95% C.L. (red dashed lines, with red-shaded regions around the 10^{-7} curve indicating the 1σ and 2σ probability bands).[3] The borders of the gray-shaded regions denote the luminosities that correspond to 1, 10, and 100 events. We see that both discovery and exclusion are expected to occur on the basis of very few events.

Observing no events when three are expected by a hypothesis is sufficient to exclude this hypothesis at 95% C.L. Thus, for luminosities that lead to a sufficiently small background $B \ll 1$, the exclusion limit corresponds to the three-event line. This is why for small $m_{\tilde{\tau}_1}$ the exclusion limits for different r_β are degenerate at the three-event line, which coincides with the $r_\beta = 10^{-10}$ line in Fig. 5—the corresponding background is sufficiently suppressed. As it is not possible to obtain less than zero events, the red-shaded regions do not continue beyond the three-event line.

In Fig. 5 we also show the results for the 7 TeV run of the LHC. The calculation has been analogous except that we have used a slightly smaller K factor of 1.3 for the normalization of the stau production cross section. We find that as the integrated luminosity exceeds an inverse femtobarn, the LHC is close to tightening the LEP bound of $m_{\tilde{\tau}_1} \gtrsim 100$ GeV, which currently remains the best limit on the direct production of long-lived sleptons. If the 7 TeV run reaches 10 fb^{-1}, one will be able to exclude stau masses up to roughly 170 GeV.

Optimized $p_{\rm T}$ cut

Looking at the $p_{\rm T}$ distribution of the staus (Fig. 4, bottom) and the $p_{\rm T}$-cut dependence of the di-muon cross section (Fig. 1, right) we see that we can improve the search by optimizing the $p_{\rm T}$ cut according to the stau mass hypothesis being considered. In other words, we repeat the previous analysis with an additional $p_{\rm T}$ cut (again on both stau candidates) that grows linearly with $m_{\tilde{\tau}_1}$,

$$p_{\rm T} > p_{\rm T}^{\min} = 0.4 \times m_{\tilde{\tau}_1}. \tag{10}$$

The stau cross section after applying this additional cut is nearly identical to the lowermost curve in Fig. 3. We emphasize that the result is not sensitive to the choice of the factor 0.4. Choosing 0.5 instead gives almost the same result.

The dependence of the background cross section on this optimized $p_{\rm T}$ cut is shown in the right panel of Fig. 1. Apart from lower statistics, in the high-$p_{\rm T}$ region we expect a larger theoretical uncertainty. Therefore we perform a conservative fit to the data, such that the fitted curve lies completely above the simulated curve in the region $p_{\rm T} > 50$ GeV.

After this change, discovery is expected to take place for one to three events in the whole considered region, as shown in Fig. 6. For instance, a scenario with a 300 GeV stau NLSP is expected to be discovered at about 10 fb^{-1} (and even for $r_\beta = 10^{-7}$ at about 20 fb^{-1}) through direct production alone. On the other hand, if it is not chosen by nature the same scenario can be excluded at 95% C.L. with roughly 30 fb^{-1}. In the very long term, nearly the whole considered mass range is accessible at the LHC, for example, masses up to 600 GeV (exclusion) and about 750 GeV (discovery) for 300 fb^{-1}. Note that the probability bands for the $r_\beta = 10^{-10}$ exclusion curve are

[3]Since even the 2σ probability band around the 10^{-10} curve is almost degenerate with the curve itself, we refrain from displaying the bands for $r_\beta = 10^{-10}$.

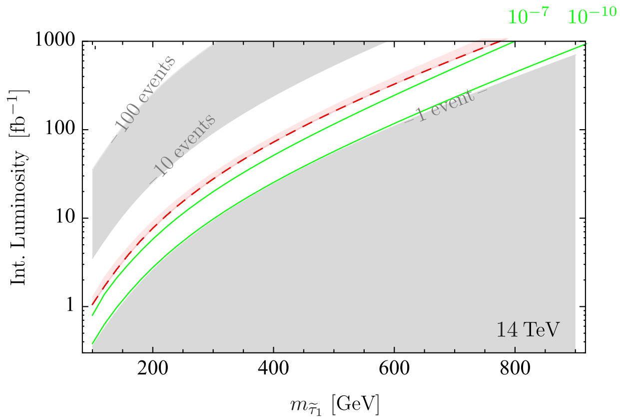

FIG. 6 (color online). Same as Fig. 5 but with an additional cut $p_T > 0.4 m_{\tilde{\tau}_1}$.

degenerate with the three-event line. In Fig. 6 only the 2σ probability band for the 10^{-7} curve is visible.

Besides, the dependence of the LHC potential on the background rejection factor r_β can be studied. The large change of r_β by 3 orders of magnitude causes only a small change in the luminosity required for a discovery by a factor of about 2. Note that the discovery curves are the expected discovery reach. Since for $r_\beta = 10^{-10}$ the sufficient event number for discovery is one or two, the statistical fluctuation is of $\mathcal{O}(1)$ too. So a discovery can easily take place at half or double the integrated luminosity shown in the figures.[4] Thus, the difference between the $r_\beta = 10^{-7}$ and $r_\beta = 10^{-10}$ discovery curve is of the same order as the expected statistical fluctuation. For this reason we assess the discovery curves to be relatively insensitive to the change in r_β in the considered range. Moreover, the exclusion limits for $r_\beta = 10^{-7}$ and 10^{-10} become degenerate at the three-event line. Thus, the exclusion potential is not sensitive to r_β at all.

This also sheds some light on the impact of the uncertainties in the background cross section. The variation of r_β over 3 orders of magnitude reveals how little impact an uncertainty of tens or even hundreds of percent in the background cross section would have. This justifies the somewhat arbitrarily chosen K factor for the muon background in Sec. II A and shows that setting the detector efficiency for the background to one was not very conservative. Similarly, it shows that our result does not rely on the exact shape of the high p_T tail of the distribution in the right panel of Fig. 1.

To realize this optimized p_T cut in an experimental analysis, one could choose the value of $p_T^{\min}$ corresponding to the stau mass that—for example, according to Fig. 6—is within reach at the luminosity of the analyzed data set.

[4]For this reason we refrain from quantizing the required event numbers to integers.

IV. DIRECT PRODUCTION VERSUS OTHER CHANNELS

The cross section for the production of superparticles heavier than the stau can be larger than the DY cross section considered so far. Such sparticles promptly decay into the NLSP, emitting standard model (SM) particles which provide an additional signature with potentially higher significance than the detection of the metastable stau. However, the SM particle radiation from cascade decays depends strongly on the sparticle mass spectrum and has to be distinguished from a higher SM background. Hence, we assume that the easiest way to find SUSY in the considered scenario is the direct detection of the NLSP, independently of its production channel. Then we can estimate whether staus from direct production or those from decays of heavier sparticles will be the dominant contribution to the discovery of a gravitino-stau scenario. This enables us to decide for which SUSY spectra our previous calculations for the direct DY production yield a good approximation for the potential of the LHC and for which spectra they are overly conservative.

We classify three sources of the production of SUSY particles,

(i) production of sleptons, including the direct production of staus,
(ii) production of neutralinos and charginos, and
(iii) production of colored sparticles.

Let us look at the leading contributions of each class. For simplicity, in each case we consider exemplary production rates of a single sparticle species and do not sum, e.g., over the generations of sfermions (which would require an assumption on the relation between their masses). It is easy to estimate the production rate in the case of degeneracies by multiplying the results by the appropriate factor. For this consideration we computed the cross section via MADGRAPH/MADEVENT 5 [44] at lowest order and cross-checked whether NLO computations [39,40,45] lead to roughly the same conclusions.

At lowest order in the electroweak coupling, $\mathcal{O}(\alpha^2)$, direct production of sleptons is only possible via neutral current and charged current DY. According to Fig. 2, right- and left-handed slepton pair production differs by a factor of about 2 in the cross section. On the other hand, such an increase of the cross section is compensated already by a rather small increase of the slepton mass by a factor of less than about 1.3. Accordingly, the contribution from another neutral current DY produced slepton $\tilde{l}_L$ decaying into the NLSP will only be noticeable if $\tilde{\tau}_1 \simeq \tilde{\tau}_R$ and for a very small gap between $m_{\tilde{\tau}_1}$ and $m_{\tilde{l}_L}$. Production of $\tilde{l}_L \tilde{\nu}_l$ via $W^\pm$ is in principle enhanced relative to $Z, \gamma \rightarrow \tilde{l}_L^+ \tilde{l}_L^-$ by a factor of 2 to 3. Since only $\tilde{l}_L$ couples to $W^\pm$, direct production of $\tilde{\tau}_1$ via $W^\pm$ is suppressed by $\sin^2\theta_{\tilde{\tau}}$ and thus unlikely for

$\tilde{\tau}_1 \simeq \tilde{\tau}_R$. By contrast, production of $\tilde{l}_L^+ \tilde{\nu}_l$ via W^+ can be of the same order as $Z, \gamma \to \tilde{\tau}_R^+ \tilde{\tau}_R^-$ if $m_{\tilde{l}_L} \simeq m_{\tilde{\nu}_l} \lesssim 1.6 m_{\tilde{\tau}_1}$. (The production via W^+ is slightly enhanced against the one via W^- due to the charge asymmetry in the initial state.) However, in any case, the production of another slepton pair $\tilde{l}^\pm \tilde{\nu}_l$ or $\tilde{l}^+ \tilde{l}^-$ decaying into a pair of $\tilde{\tau}_1$ does not have the potential to exceed the direct DY production drastically.

Production of neutralinos and charginos is accessible at $\mathcal{O}(\alpha^2)$ either via neutral and charged current DY or via t- and u-channel squark exchange. DY production of neutralinos only occurs in the case of a noticeable contribution of Higgsinos and even then the cross sections are quite small. In contrast, $Z, \gamma \to \tilde{W}^+ \tilde{W}^-$ has quite a large cross section. The same is true for $W^\pm \to \tilde{W}^\pm \tilde{W}^0$. For $m_{\tilde{W}^\pm} \lesssim 3 m_{\tilde{\tau}_R}$ the DY production of $\tilde{W}^+ \tilde{W}^-$ can exceed $Z, \gamma \to \tilde{\tau}_R^+ \tilde{\tau}_R^-$. If the charginos are more Higgsino-like the cross sections become lower; $m_{\tilde{H}^\pm} \lesssim 2 m_{\tilde{\tau}_R}$ is required for a competing or dominant Higgsino production. The production via squarks in the t and u channel introduces an additional dependence on the squark masses. However, the cross sections are roughly the same as the corresponding production via DY only if $m_{\tilde{q}} \simeq m_{\tilde{W}}$. Thus, for larger squark masses the t- and u-channel squark contributions become subleading. According to these considerations, one should keep in mind the chargino production via DY, which can become an important channel, especially in the case of a light wino.

Let us finally consider the production of colored sparticles. Since the LHC is a proton-proton collider, at leading order $\mathcal{O}(\alpha_s^2)$ squark-pair, gluino-pair, and squark-gluino production each allow a variety of diagrams that include the initial states gg, qg, and qq, which are the dominant hadronic channels at the LHC for low, middle, and high CM energies, respectively. Setting all masses equal to 1 TeV, the production of the colored sparticles and direct stau-pair production follow roughly the ratio

$$\sigma_{\tilde{q}\tilde{g}}:\sigma_{\tilde{g}\tilde{g}}:\sigma_{\tilde{q}\tilde{q}}:\sigma_{\tilde{\tau}_R^+\tilde{\tau}_R^-} \simeq 1:\frac{1}{16}:\frac{1}{33}:\frac{1}{1700}, \qquad (11)$$

where we chose $\tilde{q} = \tilde{u}$ (either right- or left-handed), which is the leading contribution. Thus, spectra with dominant direct DY production of staus are required to have quite a large mass gap between the NLSP and the colored sparticles to compensate this ratio. Large mass gaps are typical for gauge [46,47] or gaugino mediated [48,49] SUSY breaking and no-scale models [50], for example. Furthermore, (11) shows that gluino-squark production is most likely to be the dominant contribution to the production of colored sparticles.[5]

Let us close these considerations with two examples. In a scenario with

$$m_{\tilde{\tau}_R} = 200\ \text{GeV}, \qquad m_{\tilde{W}^\pm} = 600\ \text{GeV},$$
$$m_{\tilde{u}} = 1.4\ \text{TeV}, \qquad m_{\tilde{g}} = 1.8\ \text{TeV}$$

or, for a larger overall mass scale,

$$m_{\tilde{\tau}_R} = 800\ \text{GeV}, \qquad m_{\tilde{W}^\pm} = 1.7\ \text{TeV},$$
$$m_{\tilde{u}} = 2.6\ \text{TeV}, \qquad m_{\tilde{g}} = 3.2\ \text{TeV},$$

the cross sections for $\tilde{\tau}_R^+ \tilde{\tau}_R^-$, $\tilde{W}^+ \tilde{W}^-$, and $\tilde{u}\,\tilde{g}$ production are all roughly of the same size.

However, in the considered case of a rather large mass gap to the colored sparticles, the staus from cascade decays have significantly higher velocities than directly produced ones (due to the large phase space) [28,51]. Consequently, staus from cascade decays are more likely to be rejected by the velocity cut needed for the discrimination against muons. Thus, already in the exemplary equal-production-rate scenarios from above we expect direct DY production to be the dominant contribution to detectable staus.

V. CONCLUSIONS

Metastable charged supersymmetric particles lead to prominent signatures in the detectors at the LHC. We have shown that these signatures enable a very efficient background rejection. As a consequence, despite its relatively small cross section direct Drell-Yan production of metastable charged sleptons has an interesting potential for discovering or excluding their existence at the LHC for a wide range of masses. Above all, it provides a robust lower limit on the LHC potential for scenarios with a metastable charged slepton that depends only on the slepton mass. For instance, the 7 TeV run will improve the LEP limit in the near future and could exclude slepton masses up to roughly 160 GeV with an integrated luminosity of 10 fb^{-1}.

Particularly for the heavy mass range, we have proposed an additional cut depending on the slepton mass which may further reduce the background. At the 14 TeV LHC, this would allow to discover a 300 GeV stau, for example, at about 10 fb^{-1} via direct production. With a very large luminosity of 300 fb^{-1}, masses up to roughly 600 GeV could be excluded, and even heavier staus could be discovered. As mentioned, this mass region can be regarded as interesting from a cosmological point of view due to the constraints from catalyzed big bang nucleosynthesis.

In the spirit of a model-independent approach, we have assumed the stau mixing angle yielding the minimal production cross section, which is slightly below the cross section for a pure $\tilde{\tau}_R$. The limits on $\tilde{\tau}_L$ are correspondingly tighter due to its larger production cross section. Concerning experimental issues, we chose to be conservative as well. The LHC potential may improve, for example, with a better control over the distinction between charged sleptons and muons or a better detector efficiency than assumed here.

[5]As long as the masses of the squarks are not vastly different, this conclusion remains to hold if we sum over the squark flavors and vary the overall mass scale within reasonable boundaries.

By considering channels other than direct Drell-Yan production, a larger, albeit more model-dependent, discovery potential and tighter exclusion limits can be achieved. We have discussed briefly the production processes that are most likely to be the dominant ones if the mass gap between the metastable charged slepton and the heavier superparticles is not large enough to guarantee dominant Drell-Yan production. At the LHC, for many mass spectra this would be wino production or associated squark-gluino production.

ACKNOWLEDGMENTS

We would like to thank Christian Autermann, Patrick Huber, Kolja Kaschube, Boris Panes, Christian Sander, Peter Schleper, and Hartmut Stadie for very helpful discussions. We also thank CINVESTAV in Mexico City for hospitality during stages of this work. This work was supported by the German Science Foundation (DFG) via the Junior Research Group "SUSY Phenomenology" within the Collaborative Research Centre 676 "Particles, Strings and the Early Universe".

[1] P. Fayet, in *Proceedings of the 16th Rencontre de Moriond*, edited by J. Tran Thanh Van (Editions Frontieres, Gif sur Yvette, France, 1981), Vol. 1, pp. 347.
[2] H. Pagels and J.R. Primack, Phys. Rev. Lett. **48**, 223 (1982).
[3] J.R. Ellis, D.V. Nanopoulos, and S. Sarkar, Nucl. Phys. B **259**, 175 (1985).
[4] M. Bolz, W. Buchmüller, and M. Plümacher, Phys. Lett. B **443**, 209 (1998).
[5] A. Brandenburg, L. Covi, K. Hamaguchi, L. Roszkowski, and F.D. Steffen, Phys. Lett. B **617**, 99 (2005).
[6] T. Jittoh, J. Sato, T. Shimomura, and M. Yamanaka, Phys. Rev. D **73**, 055009 (2006).
[7] W. Buchmüller, K. Hamaguchi, M. Ratz, and T. Yanagida, Phys. Lett. B **588**, 90 (2004).
[8] M. Pospelov, Phys. Rev. Lett. **98**, 231301 (2007).
[9] J. Pradler and F.D. Steffen, Phys. Lett. B **666**, 181 (2008).
[10] J. Kersten and K. Schmidt-Hoberg, J. Cosmol. Astropart. Phys. 01 (2008) 011.
[11] A. Nisati, S. Petrarca, and G. Salvini, Mod. Phys. Lett. A **12**, 2213 (1997).
[12] I. Hinchliffe and F. Paige, Phys. Rev. D **60**, 095002 (1999).
[13] S. Ambrosanio, B. Mele, S. Petrarca, G. Polesello, and A. Rimoldi, J. High Energy Phys. 01 (2001) 014.
[14] S. Ambrosanio, B. Mele, A. Nisati, S. Petrarca, G. Polesello, A. Rimoldi, and G. Salvini, Rendiconti Lincei **12**, 5 (2001).
[15] J. Sjölin, Eur. Phys. J. direct C **4**, 1 (2002).
[16] J.L. Feng, S. Su, and F. Takayama, Phys. Rev. D **70**, 075019 (2004).
[17] A. De Roeck, J. Ellis, F. Gianotti, F. Moortgat, K. A. Olive, and L. Pape, Eur. Phys. J. C **49**, 1041 (2007).
[18] J.R. Ellis, A.R. Raklev, and O.K. Øye, J. High Energy Phys. 10 (2006) 061.
[19] J.L. Feng, S.T. French, C.G. Lester, Y. Nir, and Y. Shadmi, Phys. Rev. D **80**, 114004 (2009).
[20] J.L. Feng, S.T. French, I. Galon, C.G. Lester, Y. Nir, Y. Shadmi, D. Sanford, and F. Yu, J. High Energy Phys. 01 (2010) 047.
[21] J. Chen and T. Adams, Eur. Phys. J. C **67**, 335 (2010).
[22] T. Ito, R. Kitano, and T. Moroi, J. High Energy Phys. 04 (2010) 017.
[23] J.J. Heckman, J. Shao, and C. Vafa, J. High Energy Phys. 09 (2010) 020.
[24] R. Kitano and M. Nakamura, Phys. Rev. D **82**, 035007 (2010).
[25] M. Endo, K. Hamaguchi, and K. Nakaji, J. High Energy Phys. 11 (2010) 004.
[26] M. Endo, K. Hamaguchi, and K. Nakaji, arXiv:1105.3823.
[27] M. Fairbairn, A.C. Kraan, D.A. Milstead, T. Sjöstrand, P. Skands, and T. Sloan, Phys. Rep. **438**, 1 (2007).
[28] A. Rajaraman and B.T. Smith, Phys. Rev. D **75**, 115015 (2007).
[29] A. Rajaraman and B.T. Smith, Phys. Rev. D **76**, 115004 (2007).
[30] A.R. Raklev, Mod. Phys. Lett. A **24**, 1955 (2009).
[31] J. Alwall, P. Demin, S. de Visscher, R. Frederix, M. Herquet, F. Maltoni, T. Plehn, D.L. Rainwater, and T. Stelzer, J. High Energy Phys. 09 (2007) 028.
[32] T. Sjostrand, S. Mrenna, and P. Skands, J. High Energy Phys. 05 (2006) 026.
[33] J. Alwall, S. Hoeche, F. Krauss, N. Lavesson, L. Lonnblad, F. Maltoni, M.L. Mangano, M. Moretti, C.G. Papadopoulos, F. Piccinini, S. Schumann, M. Treccani, J. Winter, and M. Worek, Eur. Phys. J. C **53**, 473 (2008).
[34] J. Pumplin, D.R. Stump, J. Huston, H.L. Lai, P. Nadolsky, and W.K. Tung, J. High Energy Phys. 07 (2002) 012.
[35] C. Albajar and G. Wrochna, CERN Report No. CMS-NOTE-2000-067, 2000, http://cdsweb.cern.ch/record/687291/files/note00_067.pdf.
[36] N. Amapane, M. Fierro, and M. Konecki, CERN Report No. CMS-NOTE-2002-040, 2002, http://cdsweb.cern.ch/record/876167/files/0508194.pdf.
[37] K. Nawrocki, Proc. Sci. 2008LHC (2008) 012.
[38] CMS Collaboration, CERN Report No. CMS-PAS-EXO-08-003, 2009, http://cdsweb.cern.ch/record/1152570/files/EXO-08-003-pas.pdf.
[39] H. Baer, B. Harris, and M.H. Reno, Phys. Rev. D **57**, 5871 (1998).
[40] W. Beenakker, M. Klasen, M. Krämer, T. Plehn, M. Spira, and P.M. Zerwas, Phys. Rev. Lett. **83**, 3780 (1999); **100**, 029901(E) (2008).
[41] G. Bozzi, B. Fuks, and M. Klasen, Nucl. Phys. B **777**, 157 (2007).

[42] G. Bozzi, B. Fuks, and M. Klasen, Nucl. Phys. B **794**, 46 (2008).
[43] K. Kaschube and P. Schleper (private communication).
[44] J. Alwall, M. Herquet, F. Maltoni, O. Mattelaer, and T. Stelzer, J. High Energy Phys. 06 (2011) 128.
[45] W. Beenakker, R. Höpker, M. Spira, and P. Zerwas, Nucl. Phys. B **492**, 51 (1997).
[46] M. Dine and W. Fischler, Phys. Lett. B **110**, 227 (1982).
[47] L. Alvarez-Gaume, M. Claudson, and M. B. Wise, Nucl. Phys. B **207**, 96 (1982).
[48] D. E. Kaplan, G. D. Kribs, and M. Schmaltz, Phys. Rev. D **62**, 035010 (2000).
[49] Z. Chacko, M. A. Luty, A. E. Nelson, and E. Ponton, J. High Energy Phys. 01 (2000) 003.
[50] J. R. Ellis, C. Kounnas, and D. V. Nanopoulos, Nucl. Phys. B **247**, 373 (1984).
[51] J. Heisig and J. Kersten (in preparation).